Cahn-Hilliard Reaction Model for Isotropic Li-ion Battery Particles

Yi Zeng[1], Martin Z. Bazant[1,2]
[1]Department of Mathematics, Massachusetts Institute of Technology,
77 Massachusetts Avenue, Cambridge, Massachusetts, 02139-4307, U.S.A.
[2]Department of Chemical Engineering, Massachusetts Institute of Technology,
77 Massachusetts Avenue, Cambridge, Massachusetts, 02139-4307, U.S.A.

ABSTRACT

Using the recently developed Cahn-Hilliard reaction (CHR) theory, we present a simple mathematical model of the transition from solid-solution radial diffusion to two-phase shrinking-core dynamics during ion intercalation in a spherical solid particle. This general approach extends previous Li-ion battery models, which either neglect phase separation or postulate a spherical shrinking-core phase boundary under all conditions, by predicting phase separation only under appropriate circumstances. The effect of the applied current is captured by generalized Butler-Volmer kinetics, formulated in terms of the diffusional chemical potential in the CHR theory. We also consider the effect of surface wetting or de-wetting by intercalated ions, which can lead to shrinking core phenomena with three distinct phase regions. The basic physics are illustrated by different cases, including a simple model of lithium iron phosphate (neglecting crystal anisotropy and coherency strain).

INTRODUCTION

Intercalation compounds, such as lithium iron phosphate (Li_xFePO_4, LFP), a popular cathode material for lithium-ion batteries, present ongoing challenges for mathematical modeling. In spite of some early reported disadvantages in its conductivity and high-current capability by Padhi et al. [20], advances in surface coatings and nanoparticles have led to good cycle life and high rate capability, using a relatively low cost and environmentally friendly material. It has attracted interest for high-power applications [26, 15, 25], such as electric vehicles and hybrids [21] [28].

A striking feature of LFP is its strong tendency to separate into stable high density and low density phases, indicated by a wide voltage plateau at room temperature [20, 26] and other direct experimental evidence [11, 27, 12, 1, 19, 7]. Similar phase-separation behavior arises in many other intercalation hosts, such as graphite, the typical lithium insertion anode material, which exhibits multiple stable phases. This has inspired new approaches to model the phase separation process coupled to electrochemistry, in order to gain a better understanding of the fundamental lithium-ion battery dynamics.

The first mathematical model on two-phase intercalation dynamics in LFP was proposed by Srinivasan and Newman [23], based on the concept of a spherical “shrinking core" of one phase being replaced by an outer shell of the other phase, as first suggested by Padhi et al [20]. By assuming isotropic spherical diffusion, the sharp, radial “core-shell" phase boundary can be moved in proportion to the current. This single-particle model was incorporated into traditional porous electrode theory for Li-ion batteries [13, 18] with Butler-Volmer kinetics and concentration dependent diffusivity and fitted to experiments. The shrinking-core porous-electrode model was recently extended and refitted by Dargaville and Farrell [10].

In recent years, the shrinking-core hypothesis has been called into question since other phase behavior has been demonstrated experimentally [16, 6, 1, 12, 7] and predicted theoretically [3]. It has become clear that a more realistic particle model must account for crystal anisotropy [22, 2, 24], coherency strain [9, 8] and reaction limitation in nanoparticles [22, 2, 14] in nanoparticles. In larger, micron-sized particles, however, the shrinking-core model may still have some relevance due to solid diffusion limitation and defects (such as dislocations and micro cracks) that can reduce coherency strain. Moreover, diffusion becomes more isotropic in larger particles due to the increased frequency of point defects, such as channel-blocking Fe anti-site defects in LFP [17].

Regardless of the details of the model, fundamental questions remain about the dynamics of phase separation driven by electrochemical reactions, even in the simplest case of an isotropic strain-free spherical particle, which we consider here. When should we expect core-shell phase separation versus pure diffusion in a solid solution? What other transient phase morphologies are possible? How are reaction kinetics affected by phase separation? Traditional battery models, which place artificial spherical phase boundaries and assume classical Butler-Volmer kinetics, are not able to answer these questions.

A more accurate and consistent approach to model electrochemical kinetics with phase separation is based on non-equilibrium thermodynamics [3]. For reaction-limited anisotropic LFP nanoparticles, the general theory can be reduced to the Allen-Cahn reaction (ACR) equation for the depth-averaged ion concentration [22, 2], which has been applied successfully to predict experimental data, using generalized Butler-Volmer kinetics and accounting for coherency strain [9, 8, 3]. An important prediction of the ACR model is the dynamical suppression of phase separation [2, 9]. For large micron-sized particles, solid diffusion limitation leads to a different limit of the general theory, the Cahn-Hilliard reaction (CHR) model for bulk phase separation with heterogenous surface reactions [22, 4, 3]. The CHR model in three dimensions, however, is quite challenging to solve, and is not required to understand some of the basic physics.

In this article, we solve the CHR model with generalized Butler-Volmer kinetics for a spherical intercalation particle with concentration varying only in the radial direction. This simple one-dimensional version of the model is valid for large, defective crystals with negligible coherency strain and isotropic diffusion. It may also be directly applicable to low-strain materials such as lithium titanate, a promising long-life anode material. We simulate phase separation dynamics at constant current, which sometimes, but not always, leads to shrinking-core behavior, and we focus on the electrochemical signatures of the dynamics, which are uniquely provided by the theory [3].

ISOTROPIC CAHN-HILLIARD REACTION MODEL

In this section, we will present the basic continuum mathematical framework for ion-intercalation dynamics based on non-equilibrium thermodynamics [3]. The ion concentration profile in the bulk solid material determines the chemical potential by a Cahn-Hilliard type regular-solution model. The key innovation in the CHR model is to formulate the heterogeneous charge-transfer reaction rate via a generalized Butler-Volmer equation, which enables us to unify the concentration, current and voltage prediction from the model. Then the nondimensionalization of our system will be derived, together with an intuitive physical explanation of these nondimensional groups. Finally, we will very briefly talk about the numerical method we used for solving this system.

Model Development

The basic equation expresses mass conservation

$$\frac{\partial c}{\partial t} = -\nabla \cdot F, \tag{1}$$

where c is the concentration of the ion and F the ion flux. This ion flux is driven by the gradient of the chemical potential μ, which can be described as,

$$F = -\frac{D_0(c_m - c)c}{k_B T c_m}\nabla\mu. \tag{2}$$

Here we assume the transition state of the solid diffusion will exclude two sites, which indicates the tracer diffusivity $D = D_0(\frac{c_m - c}{c_m})$, while D_0 is the ion diffusivity and c_m is the maximum possible ion concentration within the particle.

In this model, we assume the particle is isotropic and spherical, which reduces the original 3D problem to a one-dimensional model, since the concentration now only depends on the radius dimension. For the chemical potential μ, in this model, we will use the form derived from the Cahn-Hilliard free energy functional with the regular solution model, which takes into account the contribution from pure homogeneous system and the gradient penalty. The corresponding chemical potential μ is defined as,

$$\mu = k_B T \ln\frac{c}{c_m - c} + \Omega(\frac{c_m - 2c}{c_m}) - \frac{\kappa V_s}{c_m}\nabla^2 c, \tag{3}$$

when k_B is the Boltzmann's constant, T is the absolute temperature, Ω is the enthalpy of mixing per site, κ is the gradient energy penalty coefficient, and V_s is the volume of each intercalation site. Here we will neglect the influence from the elastic strain.

At the surface of the particle, if we know the current I, by the isotropic assumption and charge conservation,

$$I = neN_A \int_A F_s dA = -4\pi R_p^2 neN_A F_s, \tag{4}$$

while R_p is the particle size in radius, F_s is the surface flux, n is the ion charge number, e is the charge of a single electron, and N_A denotes the Avogadro's number. This current condition together with the symmetric condition at the sphere center gives us the Neumann boundary condition,

$$F|_{R=0} = 0, \tag{5}$$

$$\hat{n} \cdot F|_{R=R_p} = F_s, \tag{6}$$

where $\hat{n}$ is the out-point unit normal vector. Furthermore, we impose the "natural boundary condition" for the Cahn-Hilliard equation,

$$\hat{n} \cdot (\kappa\nabla c)|_{R=R_p} = c_m^2 \frac{\partial \gamma_s}{\partial c}, \tag{7}$$

where γ_s is the surface energy per area, which generally depends on ion concentration. The natural boundary condition expresses continuity of the chemical potential and controls the tendency for a high or low concentration phase to preferentially "wet" the surface [5, 8]. These three boundary conditions suffice us to solve our model.

Dimensionless Equations

To nondimensionalize the PDE system, we will use several basic references to scale the model, which includes the particle radius R_p for the length scale, the diffusion time $\frac{R_p^2}{D_0}$ for the time scale, the maximum possible ion concentration c_m for the concentration scale and the thermal energy k_BT for any energy scale. We will follow Table 1 for each variable and parameter nondimensionalization.

Table 1: Relations for the system parameters' nondimensionalization.

$\tilde{c} = \frac{c}{c_m}$	$\tilde{t} = \frac{D_0}{R_p^2}t$	$\tilde{F} = \frac{R_p}{c_m D_0}F$	$\tilde{\nabla} = R_p\nabla$	$\tilde{\mu} = \frac{\mu}{k_BT}$	$\tilde{\Omega} = \frac{\Omega}{k_BT}$
$\tilde{\kappa} = \frac{\kappa V_s}{R_p^2 k_BT}$	$\tilde{F}_s = \frac{R_p}{c_m D_0}F_s$	$\tilde{I} = \frac{R_p^2}{neN_A D_0}I$	$\tilde{k}_0 = \frac{4\pi R_p^4}{neN_A D_0}k_0$	$\tilde{\eta} = \frac{e}{k_BT}\eta$	$\tilde{\gamma}_s = \frac{V_s}{R_p k_BT}\gamma_s$

Here $\tilde{c}$ can be seen as the local filling fraction of ions, $\frac{\tilde{\Omega}}{2}$ is the ratio of the critical temperature T_c for phase separation to the current temperature T. We will expect to have phase separation when this ratio $\frac{\tilde{\Omega}}{2} > 1$. Since $(\frac{\kappa V_s}{k_BT})^{\frac{1}{2}}$ is the length scale of the interphasial width during the phase separation, $\tilde{\kappa}^{\frac{1}{2}} = (\frac{\kappa V_s}{R_p^2 k_BT})^{\frac{1}{2}}$ is in fact the ratio of the interphasial band width scale over the particle radius scale. $\frac{1}{2}\tilde{k}_0$ is the nondimensional exchange current density when the particle is uniformly half filled while the total surface area is normalized to 4π. We will introduce this parameter k_0 in the later of this subsection. Moreover, we define a new parameter $\beta = \frac{1}{\tilde{\kappa}}\frac{\partial\tilde{\gamma}_s}{\partial\tilde{c}}$.

Then the nondimensional system can be written as,

$$\frac{\partial\tilde{c}}{\partial\tilde{t}} = -\tilde{\nabla}\cdot\tilde{F}, \tag{8}$$

$$\tilde{F} = -(1-\tilde{c})\tilde{c}\tilde{\nabla}\tilde{\mu}, \tag{9}$$

$$\tilde{\mu} = \ln\frac{\tilde{c}}{1-\tilde{c}} + \tilde{\Omega}(1-2\tilde{c}) - \tilde{\kappa}\tilde{\nabla}^2\tilde{c}, \tag{10}$$

together with the nondimensional boundary conditions,

$$\tilde{F}|_{\tilde{R}=0} = 0, \tag{11}$$

$$\hat{n}\cdot\tilde{\nabla}\tilde{c}|_{\tilde{R}=1} = \beta, \tag{12}$$

$$\hat{n}\cdot\tilde{F}|_{\tilde{R}=1} = -\tilde{F}_s, \tag{13}$$

$$\tilde{I} = -4\pi R_p^3 c_m \tilde{F}_s. \tag{14}$$

Furthermore, the reaction rate is given by Butler-Volmer equation, which enables us to relate the concentration and the current to the voltage. The parameters are again nondimensionalized by the relations in Table 1.

$$\tilde{I} = \tilde{i}_0 f(\tilde{\mu} + \Delta\tilde{\Phi}), \tag{15}$$

$$f(\tilde{\eta}) = e^{-\alpha\tilde{\eta}} - e^{(1-\alpha)\tilde{\eta}}, \tag{16}$$

$$\tilde{i}_0 = \tilde{k_0}\sqrt{\tilde{c}(1-\tilde{c})}e^{(\tilde{\Omega}(1-2\tilde{c})-\tilde{\kappa}\nabla^2\tilde{c})/2} = \tilde{k_0}(1-\tilde{c})e^{\frac{\tilde{\mu}}{2}}, \tag{17}$$

i_0 is the exchange current, η is the surface overpotential, $\Delta\Phi$ is the cathodic potential drop across the particle surface, and α is the Butler-Volmer parameter.

Numerical Scheme

In solving this PDE system, we will employ a new numerical scheme similar to the finite volume method. This new numerical method can provide us immediately the concentration on the node point but still conserve mass. Compare to the finite volume method, another major difference is the discretized equations system has a tri-diagonal mass matrix, instead of a diagonal matrix in the finite volume method.

As in the model we are mostly focusing on the activities exactly on the particle surface, the finite volume method can only provide us information about the average concentration in the shell closed to the surface, our scheme will have a great advantage in avoiding extrapolation step in the finite volume method for both surface concentration and chemical potential. After obtaining the spatial discretization of the PDE system, we employ the implicit ODE solver "ode15s" in MATLAB for the time integration. The detailed derivations of the numerical scheme can be found in the full article of this project [29].

SOLID SOLUTION

When the particle repulses the new added ions, or even the particle attracts the ions, but the temperature is higher than the critical temperature $T_c = \frac{\Omega}{2k_B}$, we would not expect any phase separation. In this case, our ion intercalation system is only a simple nonlinear diffusion process of the ion. We will focus on the simulation results from the lithiation dynamics (the discharging case). A more detailed study on both lithiation and delithiation dynamics can be found in the full article of this work [29].

In this section, we will present the concentration distribution within the sphere over time during the ion intercalation when the phase separation does not occurr, both the repulsion $\frac{\Omega}{2k_BT} < 0$ and the attraction $0 < \frac{\Omega}{2k_BT} < 1$ cases. We will also provide the voltage prediction plots during this ion intercalation process with different currents.

Table 2: Parameter settings for the numerical simulation for the case of repulsive ionic interactions, $\Omega < 0$. The same parameters settings are used to model a phase separating material with attractive interactions, $\Omega > 0$, motivated by $LiFePO_4$ reported in [2, 9].

Parameter	Value	Unit	Parameter	Value	Unit
R_p	1×10^{-7}	m	Ω	-5.14×10^{-2}	eV
κ	3.13×10^{9}	eV/m	D_0	1×10^{-12}	m^2/s
$C_{Initial}$	10	mol / m^3	C_{max}	2.29×10^{4}	mol / m^3
$c_m \frac{\partial \gamma_s}{\partial c}$	0	eV/m^2	α	0.5	-
$\Delta\Phi_a$	-3.42	V	k_0	1000	A/m^2

Solid Solution with Repulsive Forces

When $\Omega < 0$, the enthalpy in the regular solution model describes a mean-field repulsion between intercalated ions, or equivalently, an attraction between ions and vacancies, which tends to promote mixing. The enthalpic contribution to the chemical potential is then proportional to the ion

concentration. We use the following parameter setting in Table 2 to run the numerical simulation of the PDE system. Here we assume no surface wetting, which is equivalent to $\beta = 0$.

With this setting, the nondimensional $\tilde{\Omega} = \frac{\Omega}{k_B T} = -2$. When the current is small, the numerical simulations show that the ion is almost uniformly distributed inside the particle during the ion insertion process. While the current is relatively large, the diffusion of ion is slower than the ion intercalation, we see a higher ion concentration closed to the surface $\tilde{x} = 1$. This is similar to a simple spherical diffusion without any phase transition, just as expected. In the simulation, we always drive the system with a constant current. A detailed demonstration of this concentration dynamics is shown in Figure 1. The overall filling fraction X is defined as the average nondimensional concentration of the particle,

$$X = \frac{\int c dV}{\frac{4}{3}\pi R_p^3 c_m}. \tag{18}$$

We can easily see a uniform filling without any phase separation.

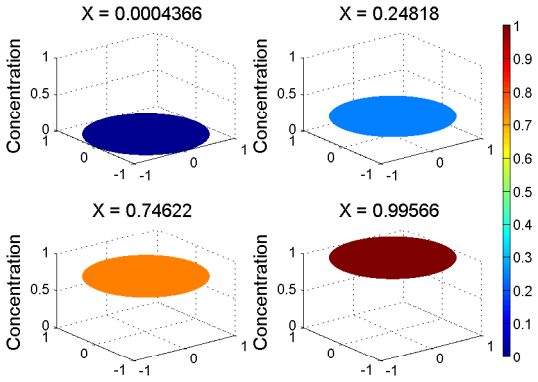

Figure 1: Solid solution with repulsive forces ($\tilde{\Omega} = -2$) ion distribution plots with different overall filling fractions. The vertical dimension in the plots shows the concentrations, while the horizontal circle denotes the hyperplane cut at the equator of the sphere. The nondimensional current $i/i_0 = 0.25$ and the X in the plot represents the overall filling fraction of lithium ion.

Given the Butler - Volmer parameter $\alpha = 0.5$, the total voltage drop between anode and particle surface can be obtained by,

$$\Delta E = \Delta\Phi - \Delta\Phi_a = -\Delta\Phi_a + \frac{k_B T}{e}(-\tilde{\mu} - 2\sinh^{-1}(\frac{\tilde{I}}{2\tilde{I}_0(\tilde{c})})) \tag{19}$$

while $\Delta\Phi$ is the cathodic potential drop across the particle surface defined before, $\Delta\Phi_a$ is the anode potential drop, and $\tilde{I}_0(\tilde{c})$ is the exchange current at the given concentration profile. Here we assume that $\Delta\Phi_a$ is always a constant. We always drive the system with a constant current. The voltage is lower when we use a higher current and we observe no voltage plateau with any of these currents. This is mainly because that a larger current will enhance the lithium ion concentration at the surface. Meanwhile, a larger running current will also lead to a larger activation potential drop, which will further decrease the total voltage. The plot of results is shown in Figure 2.

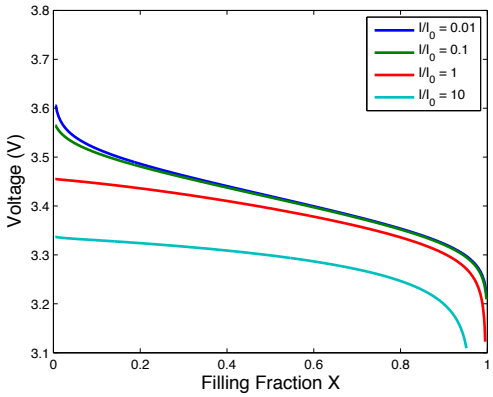

Figure 2: Solid solution with repulsive forces ($\tilde{\Omega} = -2$) voltage vs. filling fraction plot with different currents. The reference current density $i_0 = 500\ A/m^2$ is the exchange current density when particle is uniformly half filled. Four curves from top to bottom in the figure represent four different currents $i/i_0 = 0.01$, 0.1, 1 and 10 respectively.

Solid solution with Attractive Forces

When the mixing enthalpy per site Ω is positive, there are attractive forces between intercalated ions, or equivalently, repulsive forces between ions and vacancies, which tend to promote demixing and phase separation. However, when the temperature T is higher than the critical value T_c, we will still observe very similar behavior as the system with repulsive ion-ion forces. The critical temperature for this threshold in the regular solution model is given by $T_c = \frac{\Omega}{2k_B}$.

The numerical result from simulation in fact is consistent with our anticipation mentioned above. Here we use the same parameter as the simulation in ion repulsion system in Table 2, except for the Ω, which is set to be 2.57×10^{-2} eV, With this parameter $\tilde{\Omega} = 1$ then T is twice higher than T_c. The concentration profile is very close to the ones from ion repulsion systems shown in Figure 1, and the voltage plot is similar to Figure 2. Therefore, we do not include the figures for the ion distribution or the voltage plot.

PHASE SEPARATION WITHOUT SURFACE WETTING

In some materials such as the lithium iron phosphate, phase separation will be an important behavior in the ion intercalation process. In fact, when $\tilde{\Omega} > 2$, we can approach to such a phenomenon. This is essential in the lithium battery modeling and other applications.

In this section, we will show the simulation results from our model, both in concentrations and the voltages with different current. We may see from the results there is always a sudden phase transition with a sharp shock propagating in the particle after the phase separation, under our parameter choices. Later we will also give a good approximation of the voltage value when there exists a voltage plateau.

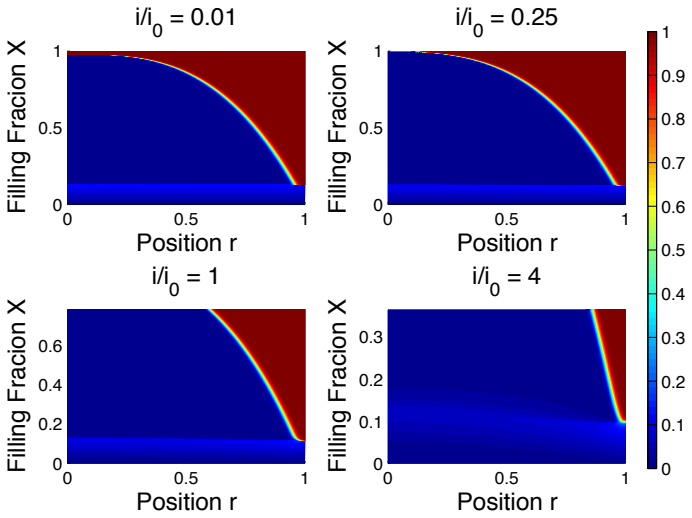

Figure 3: Phase separation system ($\tilde{\Omega} = 4.48$) concentration distributions within the spherical particle during the ion intercalation with different currents $\frac{i}{i_0} = 0.01$ (top left), 0.25 (top right), 1 (bottom left) and 4 (bottom right), while the uniformly half filled exchange current density i_0 is chosen to be 500 A/m^2. The x-axis represents the nondimensional radial position $\tilde{r}$ and the y-axis presents the overall average filling fraction X of the whole particle, which can be also seen as the time dimension. The warmer color in the figure indicates a higher local filling fraction.

Phase Separation

When the temperature is lower than the critical temperature, if we further assume the concentration is uniform, the chemical potential is then no longer a monotone function of concentration. This makes it possible for us to have a phase separation. In the simulation of this system, we again use the parameters in Table 2 but set the $\Omega = 1.15 \times 10^{-1}$ eV, which makes the $\tilde{\Omega} = 4.48 > 2$. Very different from the uniformly filling outcomes in Figure 1, the concentration profiles here with different constant currents all indicate phase separations in the concentration. Numerical results are included in Figure 3.

Indeed, the modeling results are analogous to the shrinking core model, which will create two phases section during the ion insertion. A more detailed demonstration of this phenomenon is included in the following Figure 4. But less artificially, we do not need to presume there are two regions of different phases at the beginning and we can predict when the phase separation will take place. Moreover, we do not need to solve the moving boundary problem like the shrinking core model, which makes the numerical problem more efficient to be solved.

The voltage-filling fraction curves are also quite different from the results in the previous section in Figure 2. The new results are shown in Figure 5, where we can see a sudden change in voltage when the phase separation takes place and the voltage stays on a plateau when the current is not large.

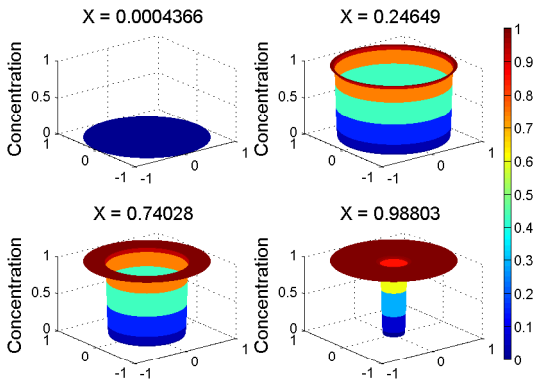

Figure 4: Phase separation system ($\tilde{\Omega} = 4.48$ and no surface wetting) ion distribution plots with different overall filling fractions. The vertical dimension in the plots shows the concentrations, while the horizontal circle denotes the hyperplane cut at the equator of the sphere. The reference current density i_0 is the exchange current density is $500\,A/m^2$ when particle is uniformly half filled. The nondimensional current $i/i_0 = 0.25$ and the X in the plot represents the overall filling fraction of lithium ion.

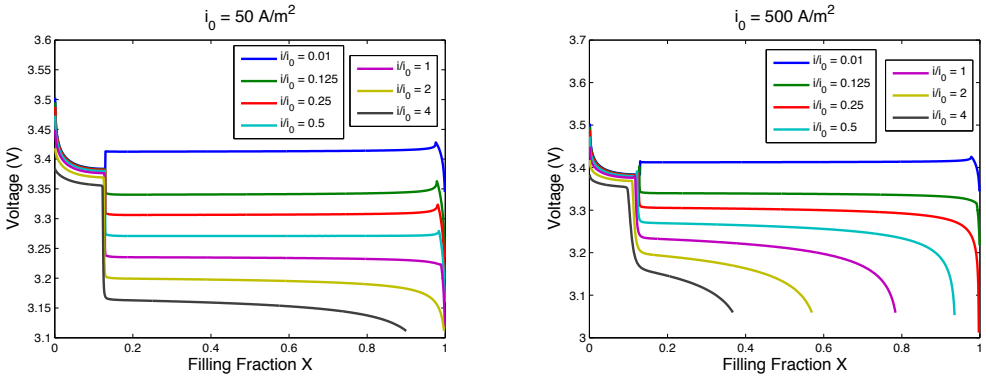

Figure 5: Phase separation system ($\tilde{\Omega} = 4.48$) voltage vs. filling fraction plot with different currents and two different reference exchange currents. The reference current density i_0 is the exchange current density which takes values $50\,A/m^2$ (left) and $500\,A/m^2$ (right) when particle is uniformly half filled.

Voltage Plateau Estimation

As we see from Figures 3, 4 and 5, under our parameter setting, we always have a phase separation in the system, which leads to a voltage plateau. In the case without surface wetting, i.e. $\beta = 0$, to approximate such voltage plateau value, we can apply the following method.

When the phase separation occurs in the case $\beta = 0$, the concentration within the highly filled phase is relatively uniform, especially when the current is not very large. Therefore, we may ignore the second order penalty term $\kappa\nabla^2 c$. Then the chemical potential approximately equals to,

$$\tilde{\mu} \approx \ln \frac{\tilde{c}}{1-\tilde{c}} + \tilde{\Omega}(1-2\tilde{c}). \tag{20}$$

When the phase separation occurs, the nondimensional concentration in each phase is approximately the root of $\tilde{\mu} = 0$. Then in the ion intercalation process, the surface concentration is approximately the larger solution $\tilde{c}_l$ of this equation. Given the nondimensional current - exchange current ratio $\xi = \frac{\tilde{I}}{\tilde{I}_0(\tilde{c}=\frac{1}{2})}$, where $\tilde{I}_0(\tilde{c} = \frac{1}{2})$ is the exchange current when the concentration $\tilde{c} = \frac{1}{2}$ throughout the whole particle, we can use the following equation to estimate the plateau voltage,

$$\Delta E = -\Delta\Phi_a + \frac{k_B T}{e}(-\tilde{\mu} - 2\sinh^{-1}(\frac{\tilde{I}}{2\tilde{I}_0})) \approx -\Delta\Phi_a - \frac{2k_B T}{e}\sinh^{-1}.(\frac{\xi}{4(1-\tilde{c}_l)}). \tag{21}$$

The comparison of the actual voltage plot and the plateau estimation from the above equation is shown in Figure 6. The results show when we are in a region of low current, the predictions fit well to the numerical simulation results.

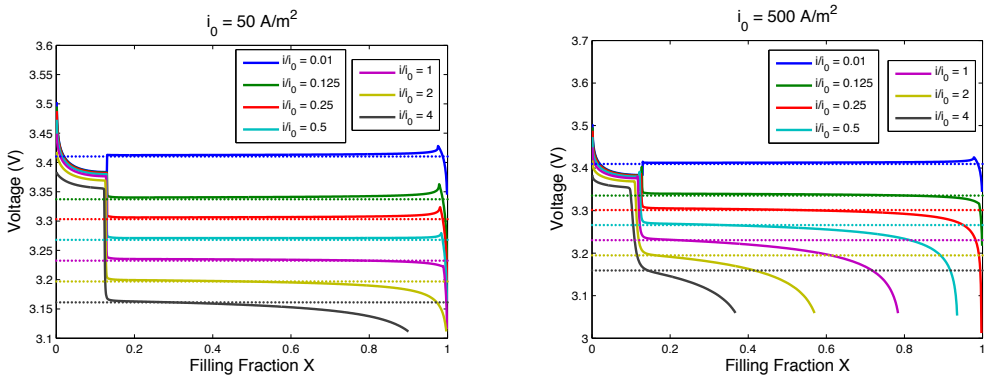

Figure 6: The comparison of real simulations of voltage in Figure 5 and the estimations of the voltage plateau in phase separation. The approximation results are shown in the dash lines.

The voltage plateau formula can be understood physically as follows. As a result of our assumption of spherical symmetry, the intercalation reaction must proceed into the outer "shell phase". In the case of lithiation, the shell has high concentration and thus strong entropic constraints inhibiting further insertion that lower the reaction rate, increase the overpotential, and lower the voltage plateau when phase separation occurs. In contrast, when the phase boundary is allowed to move along the surface as an intercalation wave [22], insertion occurs with higher exchange current at intermediate concentrations, although the active area is reduced, which leads to suppression of surface phase separation at high currents [2, 9].

PHASE SEPARATION WITH SURFACE WETTING

The surface wetting, which is the property that the ion tends or avoids to stay at the surface, may significantly change the dynamics of the ion intercalation process. In this section, we will show how the surface wetting affects the concentration and voltage during the ion insertion, with a focus on the the de-wetting case, which may create more than two stable phase regions inside the particle.

The surface wetting or de-wetting condition can be analytically expressed by the following formula,

$$\hat{n} \cdot \tilde{\nabla}\tilde{c}|_{\tilde{R}=1} = \beta, \tag{22}$$

here we no longer assume β is zero. When $\beta > 0$, the ion tends to be concentrated on the surface, which is so called surface wetting. While this value is negative, we call the case as surface de-wetting. This condition determines the concentration derivative at the spherical particle surface.

When in the surface wetting case, the surface concentration will be always higher than the remain region during the ion insertion if we start from a uniform low concentration. As results, the surface hits the spinodal point earlier than other places inside the particle, which means the Li-rich phase always nucleates at the surface. This is somehow similar to the two stable region shrinking core phenomenon in the phase separation without surface wetting system which we already discussed in the previous section.

A more interesting case takes place when we have surface de-wetting, the surface concentration derivative is negative, which is equivalent to $\beta < 0$. Since the surface concentration is always lower than the nearby concentration in the interior, especially when the current is small. Thus, the interior point will hit the spinodal concentration earlier than the surface and Li-rich phase nucleates, which differentiates itself from other previous cases.

In the numerical modeling, we set $\beta = -17.9$. This is about to set the maximum filling surface energy density of our particle to be $\gamma = -90$ mJ/m^2 in our particle size setting, if we assume the γ is a linear function of concentration. Figure 7 shows how the simulated concentration grows in this system with several currents.

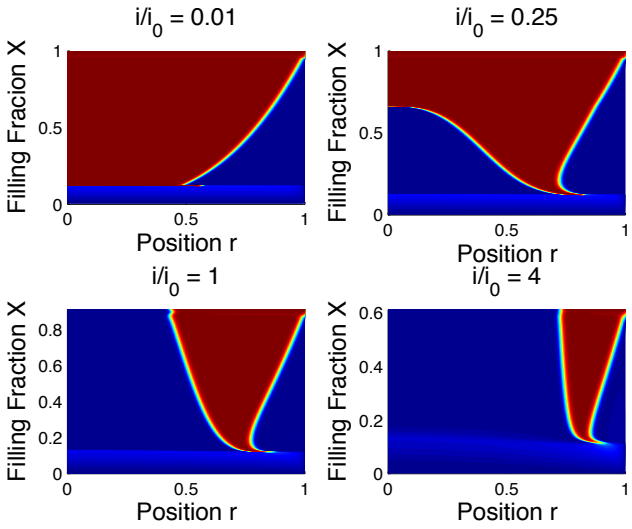

Figure 7: Concentration distributions within the surface de-wetting ($\beta = -17.9$) spherical particle during the ion intercalation with different currents $\frac{i}{i_0} = 0.01$ (top left), 0.25 (top right), 1 (bottom left) and 4 (bottom right), while the uniformly half filled exchange current density i_0 is chosen to be 500 A/m^2. The x-axis represents the nondimensional radial position $\tilde{r}$ and the y-axis presents the overall average filling fraction of the whole particle, which can be also seen as the time dimension. The warmer color in the figure indicates a higher local filling fraction.

A detailed demonstration of this concentration dynamics is shown in Figure 8. We can observe the initially uniform system later separates into three regions of two phases (Lithium rich and poor), i.e., sandwich morphology of Li poor-rich-poor three regions. The middle Li-rich region expands inward and outward simultaneously, it first fills up the Li-poor phase located at the center,

and finally it fills the whole particle. This is a prediction of shrinking core phenomenon with three phase regions. In this situation, the shrinking core model may not be easy to capture the whole concentration distribution, since we may have two or three phase regions depending on the current. The associated voltage plots of the ion insertion process in the surface de-wetting case in shown in Figure 9.

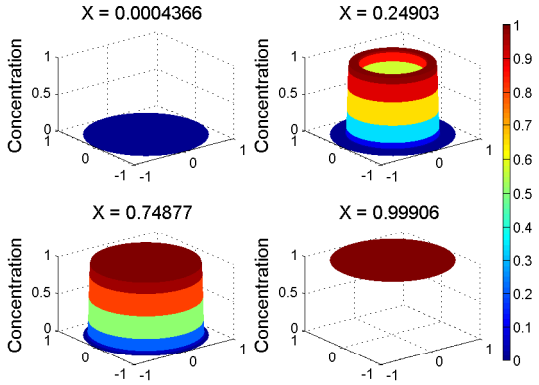

Figure 8: Phase separation system ($\tilde{\Omega} = 4.48$ and surface de-wetting $\beta = -17.9$) ion distribution plots with different overall filling fractions. The vertical dimension in the plots shows the concentrations, while the horizontal circle denotes the hyperplane cut at the equator of the sphere. The reference current density i_0 is the exchange current density is $500\,A/m^2$ when particle is uniformly half filled. The nondimensional current $i/i_0 = 0.25$ and the X in the plot represents the overall filling fraction of lithium ion.

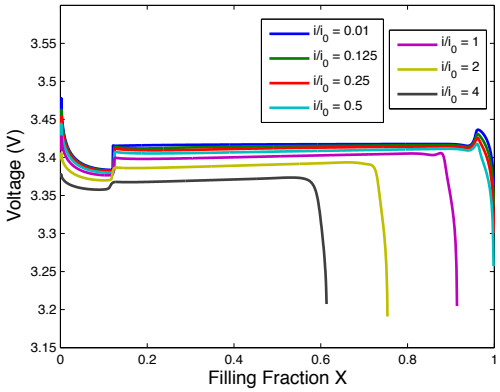

Figure 9: Strong surface de-wetting ($\beta = -17.9$) voltage vs. filling fraction plot with different current sizes $i/i_0 = 0.01$, 0.125, 0.25, 0.5, 1, 2 and 4 from top to bottom.

As we can see the surface is always in the lower stable concentration after the initial phase separation, which does not vary according to the surface derivative β, we should expect the voltage

has very weak dependence on the surface de-wetting condition. The voltage - filling fraction plot in Figure 10 actually is consistent with our intuition.

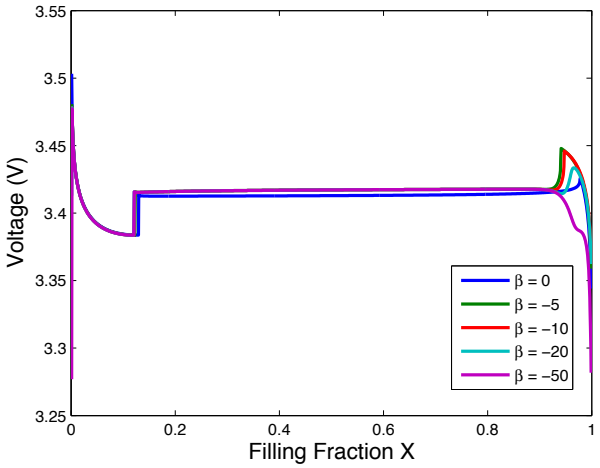

Figure 10: Surface De-wetting voltage vs. filling fraction plot, with different negative nondimensional surface concentration derivatives β. The current is chosen to be $i/i_0 = 0.01$.

CONCLUSIONS

In summary, we have studied the dynamics of ion intercalation in an isotropic spherical battery intercalation particle using the CHR model [3]. The model predicts either solid solution with radial nonlinear diffusion or core-shell phase separation, depending on the thermodynamic, geometrical, and electrochemical conditions. The model is able to consistently predict the transient voltage after a current step, regardless of the complexity of the dynamics, far from equilibrium. Surface wetting plays a major role in nucleating phase separation. The simplifying assumptions of radial symmetry and negligible coherency strain maybe be applicable to some materials, such as lithium titanate anodes or defective lithium iron phosphate cathodes, while the basic principles illustrated here have broad relevance for intercalation materials with complex thermodynamics and multiple stable phases.

ACKNOWLEDGMENTS

This material is based upon work supported by the National Science Foundation Graduate Research Fellowship under Grant No. 1122374. This work was also partially supported by the Samsung-MIT Alliance.

Reference

[1] JL Allen, TR Jow, and J Wolfenstine. Analysis of the $FePO_4$ to $LiFePO_4$ phase transition. *Journal of Solid State Electrochemistry*, 12(7-8):1031–1033, 2008.

[2] Peng Bai, Daniel Cogswell, and Martin Z. Bazant. Suppression of phase separation in $LiFePO_4$ nanoparticles during battery discharge. *Nano Letters*, 11(11):4890–4896, 2011.

[3] M. Z. Bazant. Theory of chemical kinetics and charge transfer based on non-equilibrium thermodynamics. *Accounts of Chemical Research*, 46:1144–1160, 2013.

[4] Damian Burch and Martin Z. Bazant. Size-dependent spinodal and miscibility gaps for intercalation in nanoparticles. *Nano Letters*, 9(11):3795–3800, 2009.

[5] J. W. Cahn. Critical point wetting. *J. Chem. Phys.*, 66:3667–3672, 1977.

[6] Guoying Chen, Xiangyun Song, and Thomas Richardson. Electron microscopy study of the $LiFePO_4$ to $FePO_4$ phase transition. *Electrochemical and Solid State Letters*, 9(6):A295–A298, 2006.

[7] William C Chueh, Farid El Gabaly, Josh D Sugar, Norman C. Bartelt, Anthony H. McDaniel, Kyle R Fenton, Kevin R. Zavadil, Tolek Tyliszczak, Wei Lai, and Kevin F. McCarty. Intercalation pathway in many-particle $LiFePO_4$ electrode revealed by nanoscale state-of-charge mapping. *Nano Letters*, 13:866 – 872, 2013.

[8] D. A. Cogswell and M. Z. Bazant. Theory of coherent nucleation in phase-separating nanoparticles. *Nano Letters*, Article ASAP, 2013.

[9] Daniel A. Cogswell and Martin Z. Bazant. Coherency strain and the kinetics of phase separation in $LiFePO_4$ nanoparticles. *ACS Nano*, 6:2215–2225, 2012.

[10] S. Dargaville and T.W. Farrell. Predicting active material utilization in $LiFePO_4$ electrodes using a multiscale mathematical model. *Journal of the Electrochemical Society*, 157(7):A830–A840, 2010.

[11] Charles Delacourt, Philippe Poizot, Jean-Marie Tarascon, and Christian Masquelier. The existence of a temperature-driven solid solution in Li_xFePO_4 for $0 \leq x \leq 1$. *Nature materials*, 4(3):254–260, 2005.

[12] C. Delmas, M. Maccario, L. Croguennec, F. Le Cras, and F. Weill. Lithium deintercalation of $LiFePO_4$ nanoparticles via a domino-cascade model. *Nature Materials*, 7:665–671, 2008.

[13] Marc Doyle, Thomas F. Fuller, and John Newman. Modeling of galvanostatic charge and discharge of the lithium/polymer/insertion cell. *Journal of the Electrochemical Society*, 140(6):1526–1533, 1993.

[14] T. R. Ferguson and M. Z. Bazant. Non-equilibrium thermodynamics of porous electrodes. *J. Electrochem. Soc.*, 159:A1967–A1985, 2012.

[15] Byoungwoo Kang and Gerbrand Ceder. Battery materials for ultrafast charging and discharging. *Nature*, 458:190–193, 2009.

[16] L. Laffont, C. Delacourt, P. Gibot, M. Yue Wu, P. Kooyman, C. Masquelier, and J. Marie Tarascon. Study of the $LiFePO_4/FePO_4$ two-phase system by high-resolution electron energy loss spectroscopy. *Chem. Mater.*, 18:5520–5529, 2006.

[17] Rahul Malik, Damian Burch, Martin Bazant, and Gerbrand Ceder. Particle size dependence of the ionic diffusivity. *Nano Letters*, 10:4123–4127, 2010.

[18] John Newman and Karen E. Thomas-Alyea. *Electrochemical Systems*. Prentice-Hall, Inc., Englewood Cliffs, NJ, third edition, 2004.

[19] Gosuke Oyama, Yuki Yamada, Ryuichi Natsui, Shinichi Nishimura, and Atsuo Yamada. Kinetics of nucleation and growth in two-phase electrochemical reaction of $LiFePO_4$. *J. Phys. Chem. C*, 116:7306–7311, 2012.

[20] A.K. Padhi, K.S. Nanjundaswamy, and J.B. Goodenough. Phospho-olivines as positive-electrode materials for rechargeable lithium batteries. *Journal of the Electrochemical Society*, 144(4):1188–1194, 1997.

[21] Andrew Ritchie and Wilmont Howard. Recent developments and likely advances in lithium-ion batteries. *Journal of Power Sources*, 162(2):809–812, 2006.

[22] Gogi Singh, Damian Burch, and Martin Z. Bazant. Intercalation dynamics in rechargeable battery materials: General theory and phase-transformation waves in $LiFePO_4$. *Electrochimica Acta*, 53:7599–7613, 2008. arXiv:0707.1858v1 [cond-mat.mtrl-sci] (2007).

[23] Venkat Srinivasan and John Newman. Discharge model for the lithium iron-phosphate electrode. *Journal of the Electrochemical Society*, 151(101):A1517–A1529, 2004.

[24] Ming Tang, James F. Belak, and Milo R. Dorr. Anisotropic phase boundary morphology in nanoscale olivine electrode particles. *The Journal of Physical Chemistry C*, 115:4922–4926, 2011.

[25] Ming Tang, W. Craig Carter, and Yet-Ming Chiang. Electrochemically driven phase transitions in insertion electrodes for lithium-ion batteries: Examples in lithium metal phosphate olivines. *Annual Review of Materials Research*, 40:501–529, 2010.

[26] J.M. Tarascon and M. Armand. Issues and challenges facing rechargeable lithium batteries. *Nature*, 414:359–367, 2001.

[27] Atsuo Yamada, Hiroshi Koizumi, Noriyuki Sonoyama, and Ryoji Kanno. Phase change in Li_xFePO_4. *Electrochemical and Solid-State Letters*, 8(8):A409–A413, 2005.

[28] Mats Zackrisson, Lars Avellán, and Jessica Orlenius. Life cycle assessment of lithium-ion batteries for plug-in hybrid electric vehicles–critical issues. *Journal of Cleaner Production*, 18(15):1519–1529, 2010.

[29] Yi Zeng and Martin Z. Bazant. Phase separation dynamics in isotropic ion-intercalation nanoparticles. *in preparation*, 2013.